Title	Electronic structure tuning via surface modification in semimetallic nanowires
Author(s)	Sanchez-Soares, Alfonso; O'Donnell, Conor; Greer, James C.
Publication date	2016-12-27
Original citation	Sanchez-Soares, A., O'Donnell, C. and Greer, J. C. (2016) 'Electronic structure tuning via surface modification in semimetallic nanowires', Physical Review B, 94(23), 235442. doi:10.1103/PhysRevB.94.235442
Type of publication	Article (peer-reviewed)
Link to publisher's version	http://dx.doi.org/10.1103/PhysRevB.94.235442 Access to the full text of the published version may require a subscription.
Rights	© 2016 American Physical Society
Item downloaded from	http://hdl.handle.net/10468/3498

University College Cork, Ireland
Coláiste na hOllscoile Corcaigh

Electronic structure tuning via surface modification in semimetallic nanowires

Alfonso Sanchez-Soares, Conor O'Donnell, and James C. Greer[*]

Tyndall National Institute, University College Cork, Dyke Parade, Cork T12 R5CP, Ireland

Electronic structure properties of nanowires (NWs) with diameters of 1.5 and 3 nm based on semimetallic $\alpha - $ Sn are investigated by employing density functional theory and perturbative GW methods. We explore the dependence of electron affinity, band structure, and band-gap values with crystallographic orientation, NW cross-sectional size, and surface passivants of varying electronegativity. We consider four chemical terminations in our study: methyl (CH_3), hydrogen (H), hydroxyl (OH), and fluorine (F). Results suggest a high degree of elasticity of Sn-Sn bonds within the Sn NWs' cores with no significant structural variations for nanowires with different surface passivants. Direct band gaps at Brillouin-zone centers are found for most studied structures with quasiparticle corrected band-gap magnitudes ranging from 0.25 to 3.54 eV in 1.5-nm-diameter structures, indicating an exceptional range of properties for semimetal NWs below the semimetal-to-semiconductor transition. Band-gap variations induced by changes in surface passivants indicate the possibility of realizing semimetal-semiconductor interfaces in NWs with constant cross-section and crystallographic orientation, allowing the design of novel dopant-free NW-based electronic devices.

I. INTRODUCTION

The nanopatterning of solids has been shown to induce significant variations in material properties with respect to their bulk counterparts as a result of quantum confinement effects and an increase in the impact of surface phenomena on the system as a whole due to their large surface-to-volume ratios. Tuning of a broad range of properties has been successfully demonstrated and the design of novel nanostructures exploiting chemical and structural modifications have allowed elucidation of numerous applications such as chemical sensors [1,2] transparent electronics [3], and tunnel field-effect transistors (TFETs) [4,5], making exploitation of size effects a way of enhancing a material's versatility by allowing some degree of tunability of its properties through geometric effects.

The study of semiconductor nanowire (NW) structures has been increasing since Wagner and Ellis [6] first proposed the vapor-solid-liquid growth mechanism and demonstrated submicron-scale wires of semiconducting materials five decades ago. More recently, with the advances in nanofabrication, NWs with diameters as low as 1 nm have been experimentally realized [7] and their measured band gaps reproduced by GW-corrected density functional theory (DFT) calculations [8,9]. Analogous to band-gap *widening* observed in semiconductors, bulk semimetals' electronic properties have been reported to transition to those of a semiconductor with the emergence of a band gap for structures with critical dimensions on the order of 10 nm as a result of quantum confinement with predicted band-gap values well above 1 eV in $\alpha - $ Sn NWs with diameters of approximately 1 nm [10].

Further control of NW band gaps has been reported in silicon NWs by passivating surface states with chemical groups of varying electronegativities reported to induce band-gap variations of the same order of magnitude as quantum confinement effects. Leu *et al.* [11] report variations of the order of electronvolts in Si NW band gaps when passivated

with halogens with respect to hydrogen-passivated structures, attributing reductions in band gaps to weakly interacting surface species. Nolan *et al.* [12] studied band-gap variations on similar systems passivated with NH_2 and OH and correlated band-gap variations of up to 1 eV to orbital hybridization between passivants and NW core, while Zhuo and Chou [13] correlated such band-gap reductions in Si NWs to charge redistributions and corresponding electrostatic effects induced by surface chemistry.

In the following, we explore the effects of surface passivants with varying electronegativity on NWs based on semimetallic $\alpha - $ Sn. Although not stable in bulk at room temperature [14], studies show Sn's α phase can be stabilized in thin-film structures [15–18], while $\alpha - $ Sn nanocrystals have been the focus of recent studies for applications in lithium-ion batteries [19–21]. Due to its simple crystal structure, we study $\alpha - $ Sn as a test system for exploring the range of properties that can be obtained from the competing effects of quantum confinement and chemical passivation in sub-5-nm structures based on bulk semimetals. We study the evolution with NW size and crystallographic orientation by considering structures with diameters of approximately 1.5 and 3 nm grown along low-index crystallographic orientations. NW structures have been reported to exhibit electron transport properties which makes them particularly suitable for applications in electronics [22], and, in particular, $\alpha - $ Sn NWs have been previously proposed for the design of novel nanoelectronic devices [10]. Therefore, we take a particular interest in the effects on energy band gaps—a key quantity for such applications—and improve upon the DFT description by means of a scheme based on the GW [23] approximation which has been shown to greatly improve the description of band gaps in semiconductors [24,25].

II. METHOD

Nanowire structures with cross-sectional areas corresponding to cylindrical structures with diameters of approximately 1.5 and 3 nm are modeled from bulk $\alpha - $ Sn's diamond structure (space group $Fd\bar{3}m$, no. 227). NWs oriented along

the [100], [110], and [111] crystallographic orientations are considered with their surface bonds passivated by saturating the bonding for the group-IV Sn atoms. Four different monovalent passivating groups with varying degrees of electronegativity are chosen for the study of the effects of surface passivation: methyl (-CH$_3$), hydrogen (-H), hydroxyl (-OH), and fluorine (-F). Due to the large surface-to-volume ratio in these nanostructures, a significant proportion of the Sn atoms which constitutes the NWs directly bond to the surface passivants, accounting for 40% to 44% of the chemical composition of the system as a whole in the 1.5 nm NWs, and approximately 26% to 27% in the 3 nm NWs, depending on the crystallographic orientation of a given NW.

Density functional theory (DFT) [26–28] within the usual Kohn-Sham [29] framework is employed to simulate the electronic structure of these nanostructures. We take the supercell approach for computing the properties of systems with reduced dimensionality by which at least 15 Å of vacuum is introduced along directions perpendicular to the NWs' axes in order to eliminate interactions with periodic images normal to the NWs' axes, leading to a simulation model for the NWs as infinitely long and perfectly crystalline quasi-one-dimensional systems. The Perdew-Burke-Ernzerhof (PBE) [30] formulation of the generalized gradient approximation (GGA) for the exchange and correlation functional is used in conjunction with norm-conserving pseudopotentials [31] and double-ζ-polarized basis sets of localized pseudoatomic orbitals [32,33]. Brillouin-zone integrations are performed over a grid of k points generated according to the Monkhorst-Pack [34] scheme with a density of approximately 25 k points $\times$Å along a NW axis, while real-space quantities are discretized on a grid with corresponding energy cutoffs of 200 Ry (280 Ry) for NWs passivated with hydrogen and methyl (fluorine and hydroxyl). In this approximation, the equilibrium cell parameter and bulk modulus of α − Sn are predicted to be 6.70 Å and 38 GPa, respectively. This represents a 3% deviation from experimentally reported values of 6.49 Å in the equilibrium cell parameter [15,35], and a 30% underestimation of the bulk modulus with respect to experimentally reported values of 54 GPa [36,37]. Atomic positions in the NWs are relaxed until forces acting on all atoms are below 10^{-2} eV/Å, and the total energy of the cell is minimized with respect to its length along the NW axis. Figure 1 shows cross-sectional and side views of each NW orientation and size with varying surface terminations.

Given the well-known shortcomings of standard DFT in predicting electronic band gaps [25,38,39]—a key parameter for semiconductors with applications in electronics—we improve our description through a perturbative many-body approach. We perform first-order perturbative GW [23,40,41] quasiparticle corrections for 1.5 nm NWs to gain insight into the order of magnitude of energy band gaps induced as a result of quantum confinement. Electronic structure calculations based on plane waves [42] and norm-conserving pseudopotentials [43] serve as a starting point for computing first-order corrections within the quasiparticle (QP) approximation [44] as

$$E_{nk}^{QP} = E_{nk}^{KS} + Z_{nk}\left[\Sigma_{nk}\left(E_{nk}^{KS}\right) - V_{nk}^{XC}\right], \quad (1)$$

where E_{nk}^{KS} are the Kohn-Sham eigenvalues computed from the Kohn-Sham procedure, and Σ_{nk} represents the self-energy which includes exchange and correlation effects, calculated as the convolution of one-electron Green's functions and the dynamically screened Coulomb interaction W within the plasmon-pole approximation [41]; the DFT V_{nk}^{XC} is replaced by the GW correction, and the renormalization factor—which accounts for the fact that Σ_{nk} is evaluated at Kohn-Sham eigenvalues rather than at E_{nk}^{QP}—is given by

$$Z_{nk} = \left[1 - \frac{d\Sigma_{nk}(\omega)}{d\omega}\right]^{-1}. \quad (2)$$

Plane-wave calculations for 1.5 nm structures have been performed with kinetic-energy cutoffs of 75, 90, 110, and 140 Ry for wave-function expansions in structures passivated with hydrogen, methyl, fluorine, and hydroxyl, respectively. Structural and electronic properties found in simulations performed with localized orbitals were reproduced with calculations relying on plane-wave basis sets. Given the reduced dimensionality of the systems under study, a technique for cutting off long-range Coulomb interactions has been employed when computing GW quasiparticle corrections [45].

III. RESULTS AND DISCUSSION

A. Nanowire structure

Optimal structural parameters are reported in Table I for the combinations of the Sn NW's crystallographic orientations and surface terminations studied. Small deviations in the cell parameter relative to the corresponding lattice spacing in bulk α − Sn are found for NWs passivated with atomic terminations and NWs with larger cross sections. In 1.5 nm NWs, both hydrogen- and fluorine-passivated structures exhibit lattice spacings along the NW axis within 1% of the

TABLE I. Optimized cell parameter in Å along each NW's periodic direction and characteristic cross-sectional length of Sn cores ϕ_{Sn}. Bulk column indicates cell parameter along corresponding crystallographic directions in bulk α − Sn.

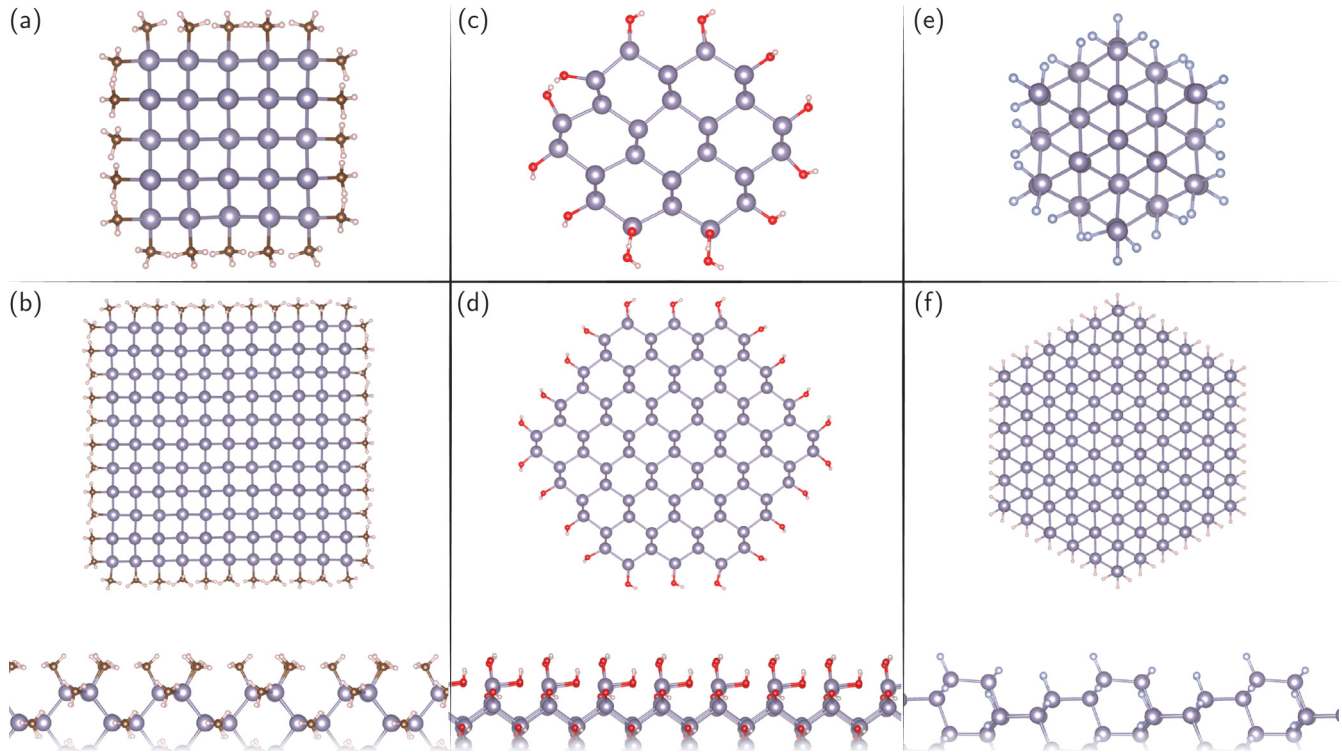|	Bulk	1.5 nm		3 nm	
	a_0 (Å)	a_0 (Å)	ϕ_{Sn} (nm)	a_0 (Å)	ϕ_{Sn} (nm)
[100]					
CH$_3$		7.00	1.35	6.87	2.95
H	6.70	6.61	1.37	6.77	2.97
OH		6.11	1.43	6.40	3.04
F		6.63	1.40	6.72	3.00
[110]					
CH$_3$		4.82	1.45	4.79	2.93
H	4.74	4.73	1.56	4.74	2.95
OH		4.71	1.58	4.74	2.96
F		4.75	1.59	4.76	2.98
[111]					
CH$_3$		11.74	1.54	11.69	3.00
H	11.60	11.52	1.50	11.62	2.98
OH		11.31	1.54	11.52	3.00
F		12.04	1.52	11.77	3.05

FIG. 1. Atomistic illustrations of Sn NW cross-sectional and side views of optimized NW structures of 1.5 nm (top row) and 3 nm (bottom row) diameters. (a),(b) [100] SnCH$_3$, (c),(d) [110] SnOH, and (e),(f) [111] SnF. Atomistic visualizations were rendered using VESTA [51].

corresponding bulk value, with the exception of the 1.5 nm [111] structures, in which an elongation of 3.8% is observed for the fluorine-passivated structure. Larger deviations relative to the corresponding bulk cell parameters are found for thinner structures and NWs passivated with molecules: cell parameters up to 4.5% larger than the corresponding bulk values are found to be induced by the larger size of the methyl molecules, while a combination of the high level of malleability of Sn-Sn bonds and the electrostatic attraction induced by the dipole moment of hydroxyl molecules at the surface favors smaller cell lengths. Despite variations in computed relaxed cell lengths encountered for different surface terminations, overall the NW's total energy displays only a remarkably weak dependence on axial strain as compared with similar strain magnitudes in the bulk.

Surface terminating groups are found to bond to surface Sn atoms without introducing significant distortions to the NW's Sn atomic structure. For surface facets exposed in [100]- and [111]-oriented structures, all terminations are found to bond to the topmost surface Sn atoms in positions exterior to the Sn core. For structures oriented along [110], there are sites in which hydroxyl and fluorine are found to align to the NW surface defined by the outermost Sn atoms as the structure is allowed to relax to a minimum-energy configuration. This results in Sn-X ($X =$ OH,F) bonds approximately parallel to the NW axis in [110]-oriented structures, as can be seen in Figs. 1(c) and 1(d). The small deviations in optimal cell lengths found for [110] NWs of 1.5 and 3 nm passivated with hydroxyl groups are attributed to this structural rearrangement, as the positioning of hydroxyl groups between Sn planes counteracts dipole attraction forces—which favor shorter cell lengths—

responsible for larger deviations in [100]- and [111]- oriented structures.

Due to variations in NW shape across structures with different crystallographic orientations, and in order to provide a unified measure of NW size, we report as cross-sectional dimensions in Table I the Sn core diameter (ϕ_{Sn}) corresponding to perfectly cylindrical structures with cross-sectional areas matching that of each NW structure, where areas have been computed by only taking Sn atoms into account to preserve comparability across surface terminations. Cross-sectional dimensions are found to remain constant across surface terminations for a given crystallographic orientation even for 1.5 nm structures, as variations reported in Table I for a given orientation and NW size correspond to differences in Sn-Sn bond lengths in directions perpendicular to the NW axis beyond the accuracy limits of our current approximation. We thus conclude that variations in relaxed cell parameters found for different surface terminations are not followed by concomitant variations in Sn-Sn bond lengths along NW cross sections.

The crystallographic orientation of the structures is found to correlate with the magnitude of maximum deviations in optimal cell parameters with respect to bulk values. NWs oriented along [100] exhibit the largest variations with molecular terminations inducing deviations of up to 4.5% and 8.8% in 1.5 nm structures, while structures oriented along [110] have the smallest deviations with a maximum of 1.7% for passivation with methyl molecules on the 1.5 nm NWs. As the cross section of the NWs increases, the magnitude of deviations in the relaxed lattice spacings decreases with the 3 nm NWs exhibiting structural parameters closer to those of bulk
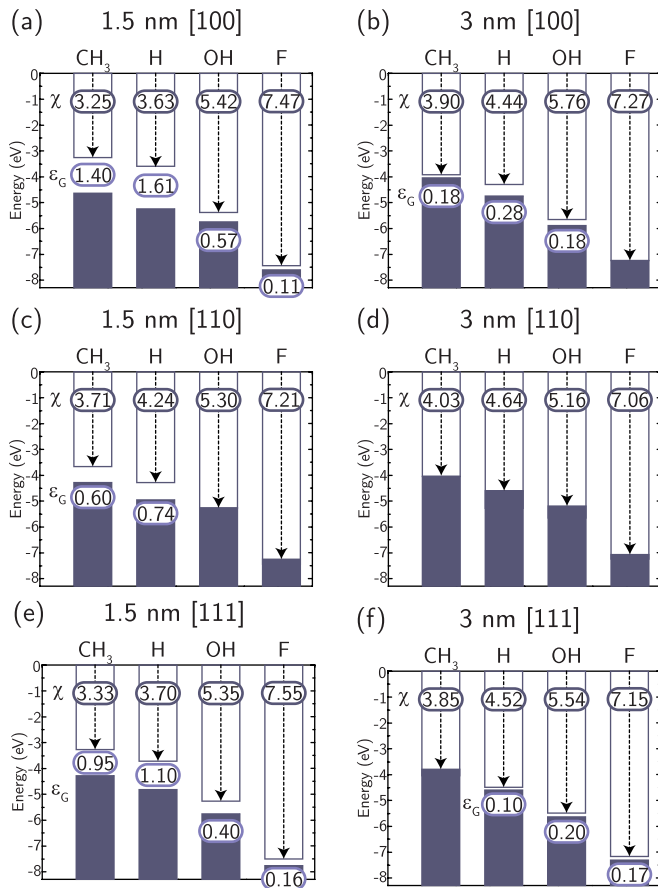
FIG. 2. Electron affinity and band gap values for 1.5 and 3 nm $\alpha -$ Sn NWs passivated and oriented along (a),(b) [100], (c),(d) [110], and (e),(f) [111] crystallographic orientations. All reported energies are in eV. Zero of energy is set to vacuum level.

$\alpha -$ Sn. This variation in structural parameters is attributed to variations in the properties of exposed surface facets with different surface terminations across structures oriented along different crystallographic axes. As NW diameter increases and the surface-to-volume ratio decreases, the impact of surface phenomena on the properties of the whole structure decreases, resulting in structural parameters rapidly approaching those of bulk $\alpha -$ Sn.

B. Electronic structure

The electronic structure of 1.5 and 3 nm $\alpha -$ Sn NWs is found to strongly depend on crystallographic orientation and surface terminations, with surface effects being more pronounced in thinner structures. Figure 2 summarizes computed DFT values for band gaps and electron affinities.

The calculations reveal that both the band gap and electron affinity can be varied for a given NW cross section and orientation via surface chemistry. Varying the surface termination groups can lead to variations in the band-gap energy on the same order of magnitude as induced by quantum confinement. Variations for the Sn NW's electron affinities are on the order of electronvolts for surface terminations considered. For confinement dimensions below 5 nm, the

potential profile confining electrons within the NWs results in a semimetal-to-semiconductor transition with the emergence of a band gap for hydrogen terminated NWs, which we take as a reference system. The potential acting on the electrons inside the Sn NW is found to be strongly related to the terminating species. As the electronegativity of the surface terminating species is increased, a shift relative to the equivalent hydrogen terminated Sn NW to the electronic energy levels towards lower values and significant reduction in the energy band-gap values occurs. This results in the NW size at which the semimetal-to-semiconductor occurs being dependent on *both* crystallographic orientation—as well as exposed surface facets along cross-sectional directions—and on the surface termination, with DFT calculations predicting variations between semimetallic behavior and energy band gaps up to 0.74 eV in 1.5 nm [110]-oriented structures by just varying surface passivants. Results show that for a given NW size and crystallographic orientation, the largest band gaps occur for hydrogen-passivated structures and the smallest band gaps for the highly electronegative case of fluorine, with values for structures passivated with other terminations following trends corresponding to the passivant's electronegativity. An exception to this trend is found for 3 nm [111] NWs: while methyl- and hydrogen-terminated structures approach semimetal behavior and exhibit band gaps below 100 meV, NWs passivated with highly electronegative species are found to exhibit larger band gaps with the fluorine-passivated structure even maintaining the magnitude of its band gap with respect to its 1.5 nm counterpart.

shows band structure plots for three representative Sn NWs. Figures 3(a) and 3(b) depict the electronic structure arising for the case of hydrogen-passivated [110] NWs in which a direct band gap at Γ is found for both 1.5 and 3 nm structures, and as anticipated from the quantum confinement effect, the magnitude reducing as the confinement dimensions increase and is reflected in the majority of Sn NWs considered in this study. Exceptions are encountered for the cases shown in Figs. 3(c)–3(f): [100] NWs passivated with hydroxyl— Figs. 3(c) and 3(d)—are found to exhibit an indirect band gap for 1.5 nm NWs, which transitions to a direct gap at Γ for the corresponding 3 nm structure, while the opposite situation is encountered in the band structures of hydroxyl- and fluorine-passivated [111] NWs, which are predicted to exhibit a direct band gap at Γ for 1.5 nm and transition to an indirect band gap for the 3 nm Sn NW, as shown in Figs. 3(e) and 3(f) for the case of fluorine. Another feature unique to [111] Sn NWs passivated with highly electronegative terminations is a gap of approximately 0.4 eV predicted to be between the conduction band and bands at higher energies, as seen in Fig. 3(e). This same feature with a gap similar in magnitude has been observed in the band structure of 1.5 nm [111] Sn NWs passivated with hydroxyl, while for less electronegative terminations, no gap is predicted within the corresponding energy range. As can be seen in Fig. 3(f), this gap reduces with increasing NW size with values of less than 40 meV in the 3 nm structures.

shows the band structure of 1.5 nm [110]-oriented NWs for all surface terminations considered. Surface-induced variations in the potential confining electrons within the NW cores are observed to interact with different bands to varying
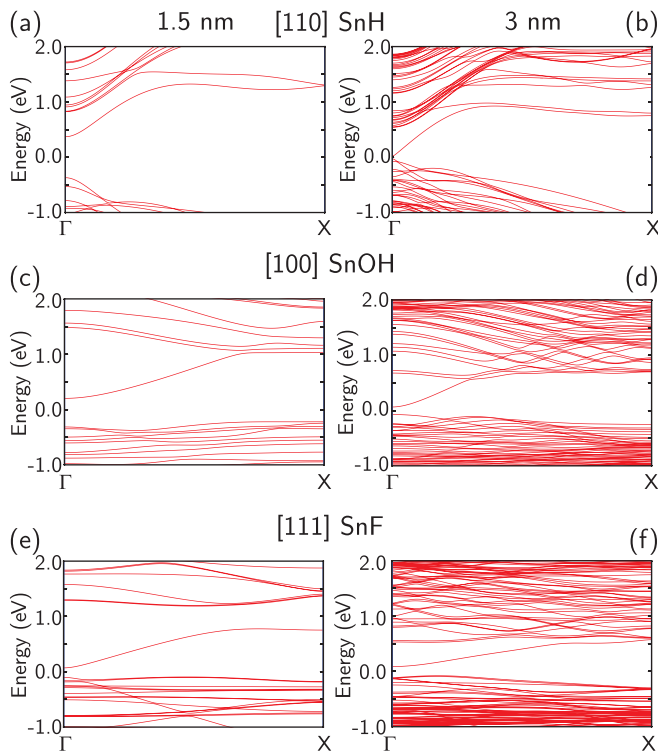
FIG. 3. Band structures of 1.5 and 3 nm $\alpha - $ Sn NWs oriented along different orientations and passivated with varying chemical species. (a),(b) [110] SnH, (c),(d) [100] SnOH, and (e),(f) [111] SnF. Zero of energy is set to the Fermi level.

FIG. 4. Band structures of 1.5 nm [110] $\alpha - $ Sn NWs passivated with varying chemical species and three-dimensional (3D) charge densities associated with valence-band maxima (bottom) and conduction-band minima (top). All charge densities taken at the same isosurface level. Zero of energy is set to the Fermi level.

degrees with larger shifts occurring in hydroxyl- and fluorine-passivated structures. Charge densities associated with the bottom of the conduction band and the top of the valence band of each structure are portrayed at the top and bottom of Fig. 4, respectively. The shown charge distributions are similar for both structures passivated with terminations with lower electronegativity values, while charge distributions for structures with more electronegative passivants are similar among them. Inspection of charge distributions corresponding to the first few bands away from the gap reveals similarities across terminations for bands with different indices; this indicates that modification of the confining potential induced by surface terminations can have an impact on band ordering, e.g., the charge distribution of the valence-band edge in hydroxyl- and fluorine-passivated structures matches that of the second topmost valence band in methyl- and hydrogen-passivated NWs. In particular, none of the structures were found to present states near the Fermi level with charge densities localized at the surface indicating proper passivation of all Sn bonds.

In order to estimate the order of magnitude of band gaps with increased accuracy, the DFT-level description is improved by means of first-order perturbative GW quasiparticle value corrections. Corrections computed across the Brillouin zone for the conduction- and valence-band edges show a dependence with k points in which the direct character exhibited by most of the structures in the study in DFT is maintained. This k dependence indicates that an explicit GW calculation is required in order to compute the full quasiparticle band
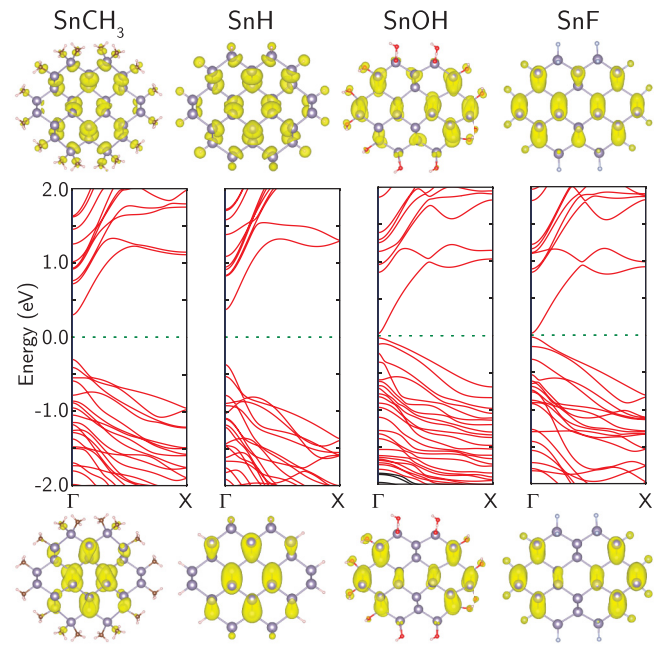
structure; in this study, we have restricted our calculations to band-gap magnitudes. Table II shows computed values of band gaps estimated using DFT with pseudoatomic orbitals (PAOs) and plane-wave (PW) basis sets, and first-order perturbative GW-corrected values for hydrogen-passivated Sn NWs of all orientations considered, and for all other surface terminations for the case of [110]-oriented NWs, which DFT predicts to exhibit the lowest band-gap values. The band-gap values predicted from approximate DFT found with both basis sets are found to be in good agreement, whereas GW corrections significantly increase the magnitude of the energy band gaps.
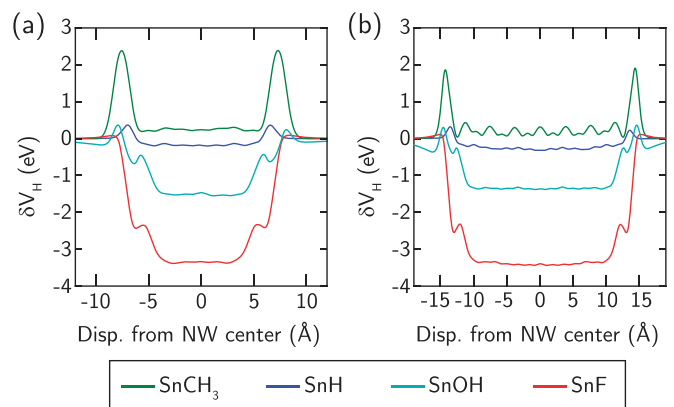

FIG. 5. Hartree difference potential profile across (a) 1.5 and (b) 3 nm NW cross sections. The depth of the induced well-like profile is found to increase with passivant electronegativity. Zero of energy has been fixed to potential values in regions far from the structures.

TABLE II. Band-gap values for 1.5 nm $\alpha - $ Sn NW structures as computed with DFT using pseudoatomic orbitals (PAOs), plane waves (PWs), and PW calculations including first-order perturbative GW quasiparticle corrections.

	DFT-PAO	DFT-PW	GW
		Band-gap energy ϵ_G (eV)	
[100]			
H	1.61	1.62	3.54
[110]			
CH$_3$	0.54	0.53	1.77
H	0.74	0.72	2.05
OH	0.02	0.02	0.25
F	0.03	0.01	0.70
[111]			
H	1.11	1.12	2.85

Even though non-self-consistent GW quasiparticle corrections are expected to underestimate energy band-gap values and depend on the starting DFT conditions, they have been shown to significantly improve upon DFT band-gap descriptions [24,46].

Trends observed in DFT across different surface passivants for [110]-oriented structure values are slightly modified after GW corrections. While structures terminated with methyl and hydrogen continue to exhibit larger band gaps than those passivated with more electronegative terminations, hydroxyl-passivated Sn NWs are predicted to exhibit a smaller energy band gap than the fluorine-passivated structure. Trends observed in DFT across crystallographic orientations for hydrogen-passivated Sn NWs are maintained after GW corrections with band gaps decreasing along the sequence $[100] - [111] - [110]$. Results indicate that $\alpha - $ Sn NWs' band-gap values can be greatly tuned with 1.5 nm structures exhibiting values ranging from 0.25 up to 3.54 eV, and variations greater than 1.5 eV achievable on single-crystalline structures by means of chemical modification. Intermediate band-gap values are expected to be possible by combining more than one surface passivant in appropriate proportions, allowing a certain degree of *band-gap engineering* to be achieved through surface chemistry [11].

C. Charge and potential

The modulation of the Sn NW electronic properties achieved by means of chemical passivation presented in the previous section is analyzed in terms of the potential and charge distributions across the NWs. To support this discussion, the electrostatics in the 1.5 and 3 nm [110] NWs is considered by examining the electron difference density $\delta n(\vec{r})$, defined as the difference in charge density between self-consistent DFT and the superposition of neutral atomic densities, and the Hartree difference potential $\delta V_H(\vec{r})$ defined as

$$\Delta \delta V_H[\delta n](\vec{r}) = -\frac{e^2}{4\pi\epsilon_0}\delta n(\vec{r}). \quad (3)$$

Figure 5 shows the Hartree difference potential across the cross section of [110] Sn NWs with diameters of 1.5 and 3 nm with different terminations averaged along a transverse axis. The profiles show potential-well profiles of varying depths depending on the electronegativity of the surface group with relatively shallow potential wells for the methyl- and hydrogen-terminated NWs relative to hydroxyl- and fluorine-terminated NWs; the latter surface terminations induce potential depths around an order of magnitude larger. The electrostatic potential flattens in regions near the center of the NWs with well depth comparable to NWs of different diameters and orientations but with the same terminating species.

Electron difference density maps $\delta n(\vec{r})$ corresponding to these potentials are shown in Fig. 6. As Mulliken population analyses [47] indicate, bonding to the Sn atoms withdraws charge from the NW onto the terminating groups according to their electronegativity, with the Mulliken charge on hydrogen and methyl increasing by 0.10–0.15 electron, and on hydroxyl and fluorine increasing by 0.5–0.6 electron. This is reflected in Fig. 6 by regions of charge accumulation at the surface (green) corresponding to the atomic positions of the surface groups. Values around the Sn core indicate an overall deficit of electrons (red) with accumulation zones around bonds between atoms and especially near surface groups. In Figs. 6(e)–6(h), green areas indicating accumulation of electrons can be seen near regions of strong charge deficit at the surface and towards the center of the NWs (i.e., *inside* the Sn core); these correspond to the situation where the surface groups bond to surface Sn atoms parallel to the NW axis, as depicted in Figs. 1(c) and 1(d) for hydroxyl-passivated [110]-oriented NW structures.

When electron withdrawal occurs at the surface of these systems, the Sn atoms' electrostatic screening results in a well-like potential profile, with the potential depth correlating to the amount of charge transfer taking place at the surface. A parallel may be drawn between these systems and the classical electrostatics problem of a charge density distributed along the surface of an infinitely long cylinder by treating electronic charge accumulation and the induced deficit in the NW core as two concentric cylindrical charge distributions. The charge distributions give rise to a potential difference between regions outside and inside both cylinders, which can be expressed as

$$\Delta\varphi = \frac{n_s}{2\pi\epsilon_0}\ln\frac{r_o}{r_i}, \quad (4)$$

where n_s is the surface charge density, r_o is the radius of the outer cylinder, r_i is the radius of the inner cylinder, and ϵ_0 is the permittivity of free space. By analogy, more electronegative passivating groups induce a larger surface charge density, thus increasing the potential difference between regions outside and inside of the NW, which results in a net lowering of the electronic states' energy and a concomitant increase in electron affinity. As discussed previously, $\Delta\varphi$ remains approximately constant across NWs with the same surface termination, which points to induced surface charge densities which do not depend on the properties of the different surface facets exposed in NWs with different crystallographic orientations, but rather on the passivant-to-Sn ratio which is approximately constant for all structures of a given diameter.

Given the charge distribution inside the NW cores and their small cross sections—of the order of the diameter of
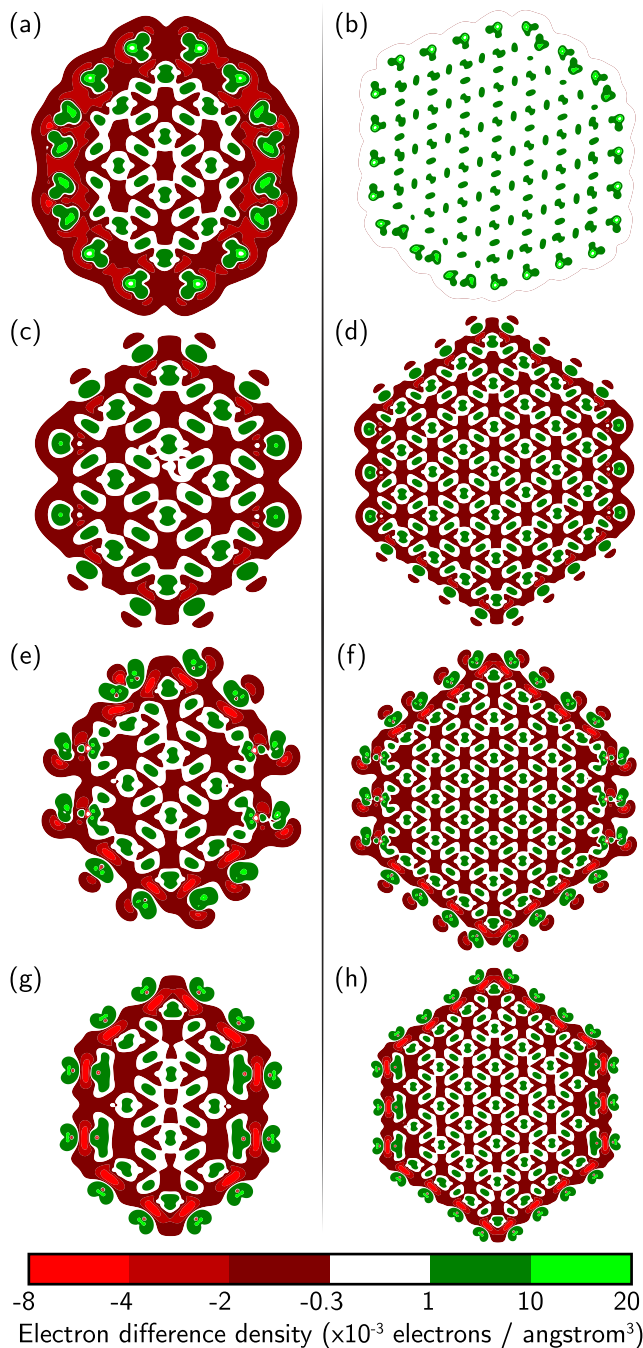
FIG. 6. Electron difference density averaged along the NW axis for 1.5 and 3 nm structures oriented along [110] and passivated with (a),(b) methyl groups, (c),(d) hydrogen atoms, (e),(f) hydroxyl groups, and (g),(h) fluorine atoms.

a benzene ring for the smaller NWs—we may analyze the effect of modifying surface electronegativity by terminating groups on NW band gaps in terms of molecular electronics arguments first proposed by Aviram and Ratner [48]. By establishing a parallel between molecules and NWs, and between substituent Hammett constants and passivant electronegativities [49], the observed trend of band-gap reduction with increasing surface termination electronegativity is as follows: the charge distribution induced by highly electronegative

surface groups results in a NW core deficient in electrons, increasing the Sn NW's electron affinity in the core, and thus lowering the energy of its conduction band—as with the lowest unoccupied molecular orbital (LUMO) in molecular rectifiers.

By extending the analogy with molecular electronics and exploiting the dependence of NW energy band gaps with surface terminations, the properties of a rectifying junction designed by abruptly switching surface groups from fluorine to hydrogen along the length of an infinitely long 1.5-nm-diameter [110]-oriented NW have been studied [50].

IV. CONCLUSION

Electronic and structural properties of highly idealized crystalline $\alpha - $ Sn NWs with diameters of approximately 1.5 and 3 nm oriented along [100], [110], and [111] directions with surface bonding saturated by chemical groups of varying electronegativity are reported. Structurally, the NWs exhibit a remarkably weak dependence in total energy with respect to the lattice spacings along the NW axes. Surface terminations were not found to induce significant surface reconstructions or modify bond lengths in directions perpendicular to the NWs' axes, although bonding schemes were found to vary somewhat with different terminating species. The calculations show a high degree of control over the NWs' band gap, and electron affinity can be achieved by varying the degree of charge transfer between NW core and surface groups by selecting the electronegativity of the latter. Charge transfer at the surface results in well-like potential profiles which increase in depth with increasing electronegativity of the surface groups, lowering the energy of electronic states inside the NW core, increasing the system's electron affinity, and reducing band-gap values in most cases. Quasiparticle corrections within a GW framework were performed to explore the range of band-gap variations showing that sub-5-nm Sn structures can range from remaining semimetallic to wide-gap semiconductors via surface chemical modification. Surface groups allow counteracting quantum confinement effects and provide further control of electronic properties, allowing significant variations of energy band-gap values along the length of structurally homogeneous Sn NW cores via variation of surface coverages. Given the suitability of NW systems' electron transport properties for the design of nanoelectronics components [22] and the broad range of band gaps found for Sn NWs, we expect semimetallic systems in the sub-5-nm size range to be strong candidates for the design of next-generation charge-based components such as rectifiers and field-effect transistors.

[1] L. Liao, Z. Zhang, B. Yan, Z. Zheng, Q. L. Bao, T. Wu, C. M. Li, Z. X. Shen, J. X. Zhang, H. Gong, J. C. Li, and T. Yu, Nanotechnology **20**, 085203 (2009).

[2] D. Kim, Y.-K. Kim, S. C. Park, J. S. Ha, J. Huh, J. Na, and G.-T. Kim, Appl. Phys. Lett. **95**, 043107 (2009).

[3] E. N. Dattoli, Q. Wan, W. Guo, Y. Chen, X. Pan,, and W. Lu, Nano Lett. **7**, 2463 (2007).

[4] Q. T. Zhao, S. Richter, C. Schulte-Braucks, L. Knoll, S. Blaeser, G. V. Luong, S. Trellenkamp, A. Schfer, A. Tiedemann, J. M. Hartmann, K. Bourdelle, and S. Mantl, IEEE J. Electron Devices Soc. **3**, 103 (2015).

[5] F. Conzatti, M. G. Pala, D. Esseni, E. Bano, and L. Selmi, IEEE Trans. Electron Devices **59**, 2085 (2012).

[6] R. S. Wagner and W. C. Ellis, Appl. Phys. Lett. **4**, 89 (1964).

[7] D. D. D. Ma, C. S. Lee, F. C. K. Au, S. Y. Tong, and S. T. Lee, Science **299**, 1874 (2003).

[8] A. J. Read, R. J. Needs, K. J. Nash, L. T. Canham, P. D. J. Calcott, and A. Qteish, Phys. Rev. Lett. **69**, 1232 (1992).

[9] X. Zhao, C. M. Wei, L. Yang, and M. Y. Chou, Phys. Rev. Lett. **92**, 236805 (2004).

[10] L. Ansari, G. Fagas, J.-P. Colinge, and J. C. Greer, Nano Lett. **12**, 2222 (2012).

[11] P. W. Leu, B. Shan, and K. Cho, Phys. Rev. B **73**, 195320 (2006).

[12] M. Nolan, S. O'Callaghan, G. Fagas, J. C. Greer, and T. Frauenheim, Nano Lett. **7**, 34 (2007).

[13] K. Zhuo and M.-Y. Chou, J. Phys.: Condens. Matter **25**, 145501 (2013).

[14] W. Paul, J. Appl. Phys. **32**, 2082 (1961).

[15] R. Farrow, D. Robertson, G. Williams, A. Cullis, G. Jones, I. Young, and P. Dennis, J. Cryst. Growth **54**, 507 (1981).

[16] H. Höchst and I. Hernández-Calderón, Surf. Sci. **126**, 25 (1983).

[17] P. John, T. Miller, and T.-C. Chiang, Phys. Rev. B **39**, 3223 (1989).

[18] K. Ueda, H. Nakayama, M. Sekine, and H. Fujita, Vacuum **42**, 547 (1991).

[19] H. S. Im, Y. J. Cho, Y. R. Lim, C. S. Jung, D. M. Jang, J. Park, F. Shojaei, and H. S. Kang, ACS Nano **7**, 11103 (2013).

[20] S. Küfner, J. Furthmüller, L. Matthes, M. Fitzner, and F. Bechstedt, Phys. Rev. B **87**, 235307 (2013).

[21] N. Oehl, L. Hardenberg, M. Knipper, J. Kolny-Olesiak, J. Parisi, and T. Plaggenborg, Cryst. Eng. Comm. **17**, 3695 (2015).

[22] J. Appenzeller, J. Knoch, M. T. Bjork, H. Riel, H. Schmid, and W. Riess, IEEE Trans. Electron Devices **55**, 2827 (2008).

[23] L. Hedin, Phys. Rev. **139**, A796 (1965).

[24] M. van Schilfgaarde, T. Kotani, and S. Faleev, Phys. Rev. Lett. **96**, 226402 (2006).

[25] M. Grüning, A. Marini, and A. Rubio, J. Chem. Phys. **124**, 154108 (2006).

[26] R. M. Dreizler and E. K. Gross, *Density Functional Theory: An Approach to the Quantum Many-Body Problem* (Springer, Berlin, 1990).

[27] J. M. Soler, E. Artacho, J. D. Gale, A. Garcia, J. Junquera, P. Ordejon, and D. Sanchez-Portal, J. Phys.: Condens. Matter **14**, 2745 (2002).

[28] Computer code Atomistix ToolKit, version 2015-1 (Quantum-Wise A/S, Denmark), www.quantumwise.com (unpublished).

[29] W. Kohn and L. J. Sham, Phys. Rev. **140**, A1133 (1965).

[30] J. P. Perdew, K. Burke, and M. Ernzerhof, Phys. Rev. Lett. **77**, 3865 (1996).

[31] I. Morrison, D. M. Bylander, and L. Kleinman, Phys. Rev. B **47**, 6728 (1993).

[32] T. Ozaki, Phys. Rev. B **67**, 155108 (2003).

[33] T. Ozaki and H. Kino, Phys. Rev. B **69**, 195113 (2004).

[34] H. J. Monkhorst and J. D. Pack, Phys. Rev. B **13**, 5188 (1976).

[35] J. Thewlis and A. R. Davey, Nature (London) **174**, 1011 (1954).

[36] C. J. Buchenauer, M. Cardona, and F. H. Pollak, Phys. Rev. B **3**, 1243 (1971).

[37] H. Kamioka, Jpn. J. Appl. Phys. **22**, 1805 (1983).

[38] J. P. Perdew, R. G. Parr, M. Levy, and J. L. Balduz, Phys. Rev. Lett. **49**, 1691 (1982).

[39] J. P. Perdew and M. Levy, Phys. Rev. Lett. **51**, 1884 (1983).

[40] A. Marini, C. Hogan, M. Grüning, and D. Varsano, Comput. Phys. Commun. **180**, 1392 (2009).

[41] F. Aryasetiawan and O. Gunnarsson, Rep. Prog. Phys. **61**, 237 (1998).

[42] P. Giannozzi, S. Baroni, N. Bonini, M. Calandra, R. Car, C. Cavazzoni, D. Ceresoli, G. L. Chiarotti, M. Cococcioni, I. Dabo, A. D. Corso, S. de Gironcoli, S. Fabris, G. Fratesi, R. Gebauer, U. Gerstmann, C. Gougoussis, A. Kokalj, M. Lazzeri, L. Martin-Samos, N. Marzari, F. Mauri, R. Mazzarello, S. Paolini, A. Pasquarello, L. Paulatto, C. Sbraccia, S. Scandolo, G. Sclauzero, A. P. Seitsonen, A. Smogunov, P. Umari, and R. M. Wentzcovitch, J. Phys.: Condens. Matter **21**, 395502 (2009).

[43] N. Troullier and J. L. Martins, Phys. Rev. B **43**, 1993 (1991).

[44] M. S. Hybertsen and S. G. Louie, Phys. Rev. B **34**, 5390 (1986).

[45] C. A. Rozzi, D. Varsano, A. Marini, E. K. U. Gross, and A. Rubio, Phys. Rev. B **73**, 205119 (2006).

[46] M. van Schilfgaarde, T. Kotani, and S. V. Faleev, Phys. Rev. B **74**, 245125 (2006).

[47] R. S. Mulliken, J. Chem. Phys. **23**, 1833 (1955).

[48] A. Aviram and M. A. Ratner, Chem. Phys. Lett. **29**, 277 (1974).

[49] L. Liu, Y. Fu, R. Liu, R.-Q. Li, and Q.-X. Guo, J. Chem. Inf. Comput. Sci. **44**, 652 (2004).

[50] A. Sanchez-Soares and J. C. Greer, Nano Lett. **16**, 7639 (2016).

[51] K. Momma and F. Izumi, J. Appl. Crystallogr. **44**, 1272 (2011).